

## Article

# Uptake and Cellular Effects of Polymethylmethacrylate on Human Cell Lines

Arthur Braun and Harald Seitz \* 

Fraunhofer Institute for Cell Therapy and Immunology, Branch Bioanalytics and Bioprocesses, 14476 Potsdam, Germany; arthur.braun@izi-bb.fraunhofer.de

\* Correspondence: harald.seitz@izi-bb.fraunhofer.de; Tel.: +49-331-58187-208

**Abstract:** The usage of plastic and its decomposition products leads to their ubiquitous distribution, resulting in their uptake by all living beings, including humans. Polymethylmethacrylate (PMMA) is known as a biocompatible polymer and is used widely in medicine and dentistry, although recent findings have shown its induction of oxidative stress within cells. Worryingly, hardly any data exist investigating the uptake of PMMA particles by cells, the potential effects of these particles on cells and cell signaling pathways and their contributing factors. We assessed the uptake of PMMA beads via confocal microscopy after their incubation with HEK293, A549 and MRC5 cells. Through cell staining, we localized multiple PMMA beads within the cytosol of cells. No alterations regarding cell growth, cell morphology or cell division were found, implying no short-term toxicity towards human cells. Using a cAMP response element binding protein (CREB)-mediated reporter assay, we assessed whether internalized PMMA nanobeads alter cell signaling pathways after stimulation of the cells. CREB was chosen as a well-described transcription factor involved in various cellular processes. Our data led to the assumption that PMMA nano- and microbeads are internalized via endocytosis and end up in lysosomes within the cell cytosol. We concluded that differences regarding the surface composition of the PMMA nanobeads affect their potential to alter cell signaling. These findings emphasize the key role the surface composition plays regarding microplastics and their risks for human health, whereas the usage of medical-grade PMMA remains safe.

**Keywords:** CREB; PMMA; microplastics; confocal microscopy; nanoplastics



**Citation:** Braun, A.; Seitz, H. Uptake and Cellular Effects of Polymethylmethacrylate on Human Cell Lines. *Microplastics* **2024**, *3*, 205–216. <https://doi.org/10.3390/microplastics3020012>

Academic Editors: Javier Bayo and Nicolas Kalogerakis

Received: 24 November 2023

Revised: 12 January 2024

Accepted: 2 April 2024

Published: 5 April 2024



**Copyright:** © 2024 by the authors. Licensee MDPI, Basel, Switzerland. This article is an open access article distributed under the terms and conditions of the Creative Commons Attribution (CC BY) license (<https://creativecommons.org/licenses/by/4.0/>).

## 1. Introduction

Despite all efforts to reduce plastic use and increase recycling, the amount of plastic produced annually still increases [1]. Both the decay of waste as well as the intentional usage of microplastics (<5 mm) has led to their ubiquitous distribution around the world [2–4]. Microplastics are present in drinking water, air and food. Furthermore, microplastics can act as vectors for harmful chemicals and pathogens, imposing additional threats to human health [5]. Upon uptake, microplastics induce inflammation, neurotoxicity, oxidative stress and changes in the metabolome in eukaryotic organisms [3,6,7]. Polymethylmethacrylate (PMMA) is a synthetic polymer of which its usefulness derives from two properties. Being a transparent thermoplastic polymer has enabled its widespread use as a shatterproof alternative to glass; thus, it is also known as “acrylic glass”. Remarkably, PMMA is also known as a biocompatible polymer with low toxicity, allowing for its use in medicine, dentistry and cosmetics [8,9]. Applications in the medical field involve its use as “bone cement” for the fixation of prosthetics, and as a base material for contact lenses and dentures. In addition, various drug delivery systems for use in humans based on PMMA nanobeads have been described and are currently being researched for a variety of applications [9–12]. Lastly, PMMA nanobeads are added to medical and cosmetic creams for application on human skin. Be it through the release of PMMA particles due to friction in prosthetics or the targeted application as a drug delivery system or cream, the uptake of PMMA particles is

inevitable. While it is known that PMMA nanobeads can induce oxidative stress in human cell lines, hardly any data exist regarding the risks the uptake of PMMA and contributing factors harbor for human health [13]. Studies have already proven that humans ingest nano- and microplastics from various sources resulting in an accumulation within the lungs, kidney and liver [14]. Recently, it was also shown that, after ingestion, microplastics are detected in human urine. This means that these particles are adsorbed via the digestive tract or pulmonary diffusion and excreted via the kidney [15]. For that reason, the lungs, kidneys and the liver are especially prone to harmful effects after ingestion. Therefore, cell lines and 3D cell models resembling the functionality of these organs are of special interest. We used confocal imaging techniques to investigate if PMMA nano- and microbeads are internalized by HEK293, A549 or MRC5 cells or remain at the surface of cells or in the media. Furthermore, we analyzed the influence of PMMA beads on signal transduction pathways. With the addition of PMMA resulting in abolished cAMP response element binding protein (CREB)-mediated in vitro transcription, altered CREB signaling after the uptake of PMMA by human cells is expected [16]. CREB is a ubiquitously expressed transcription factor and is essential for the function of a cell. CREB-mediated signaling regulates eukaryotic signaling processes, especially in the development of long-term memories and the regulation of the cell cycle [17]. CREB is part of the protein kinase A (PKA) signaling pathway, with it mainly being activated through phosphorylation. Disturbances regarding CREB-mediated signaling can result in defective neuronal development, abolished hematopoiesis and play a role in the development of cognitive and neurodegenerative disorders [18,19]. The aim of this study was to visualize the uptake of PMMA by human cell lines. With the emerging research linking the uptake of microplastics to neurodegenerative disorders, we also investigated whether PMMA particles will alter CREB-mediated signaling as a possible mechanism behind it [20].

## 2. Materials and Methods

### 2.1. Cell Culture

HEK293 and A549 cells (DSMZ, Braunschweig, Germany) were cultivated in DMEM (Sigma-Aldrich, Taufkirchen, Germany), while MRC5 cells (ATCC, Manassas, VA, USA) were cultivated in Alpha-MEM (Biowest, Nuaille, France) with 10% fetal bovine serum added (Biowest, Nuaille, France) at 37 °C, 5% CO<sub>2</sub>. Every two to three days, cells were passaged to not exceed 80% confluency. Doubling times were determined to assess whether PMMA beads reduced cell growth and division. Using a 24-well plate (Sarstedt, Germany), 5 × 10<sup>4</sup> cells per well were incubated with 12.5 µg/mL or 1.25 µg/mL PMMA for 72 h. After 72 h of incubation, cell nuclei were stained for 20 min with a phosphate-buffered saline (PBS) solution containing 5 µg/mL Hoechst 33,342 (Abcam, Cambridge, UK). For image acquisition, cells were then placed in the fluorescence microscope IX83 from Olympus (Tokyo, Japan), whereby the microscope software “scanR” (<https://www.olympus-lifescience.com/en/microscopes/inverted/scanr/>) enabled cell counting using the pictures acquired after staining the cell nuclei. For sufficient accuracy and subsequent statistical analysis, 25 images for each well were acquired to determine the cell number. Using the following equation, the doubling time ( $t_D$ ) was calculated:

$$t_D = \frac{\log_{10}(2) * \text{incubation time [h]}}{\log_{10} N - \log_{10} N_0}$$

with  $N_0$  being the number of cells at the start and  $N$  after 72 h.

### 2.2. Confocal Imaging

For confocal imaging, HEK293, A549 and MRC5 cells were seeded out in an eight-well chambered coverslip (ibidi, Gräfelfing, Germany) with each well containing 2 × 10<sup>4</sup> cells and 4.5 × 10<sup>9</sup> beads/mL. After incubation for 48 h, cells were fixed with 4% (*m/v*) paraformaldehyde for 15 min, washed two times with PBS and then stained for 30 min using a PBS solution containing 5 µg/mL Hoechst 33,342 and 200 µg/mL Concanavalin

A (Con A)-Alexa Fluor™ 594 (ThermoFisher, Hennigsdorf, Germany). Hoechst 33,342 is a fluorescent dye used to stain the nucleus, while Con A binds to carbohydrates mainly found on the cell membrane. After staining, cells were washed with PBS to minimize unspecific signals during image acquisition. Images were collected using a LSM 710 from Zeiss (Jena, Germany) at 40×/63× magnification. Image analysis was performed via ImageJ 1.54b software.

### 2.3. Transfection of HEK293 Cells

HEK293 cells were plated at a density of  $3 \times 10^4$  per well in a 24-well plate with PMMA nanobeads ( $4.5 \times 10^9$  beads/mL). After 72 h, cells were transfected with either one of the following plasmids: CMV-MGFP as the positive control, CRE-MGFP as the inducible gene and TATA-MGFP linked to a non-inducible region as the negative control [16]. All three plasmids are part of a Cignal Reporter Assay Kit (Qiagen, Venlo, The Netherlands) and based on the stimulation of a CREB-mediated protein kinase A (PKA) signaling pathway. The principle of transfection is lipotransfection. Transfection was performed according to the manufacturer's instruction (TransIT®-293 Reagent, Mirus Bio LLC, Madison, WI, USA). After 24 h, the transfection is finished, and the cells were washed with PBS. Prior to the stimulation, the cells were incubated with DMEM lacking fetal calf serum for 2 h. For stimulation, 50 µM forskolin (Merck, Darmstadt, Germany) and 50 µM 3-Isobutyl-1-methylxanthin (IBMX, Merck, Darmstadt, Germany) were then added. Forskolin activates adenylyl cyclases, resulting in increased intracellular cAMP levels. IBMX is a nonspecific inhibitor of phosphodiesterase, thus inhibiting the breakdown of cAMP. This leads to the long-term activation of protein kinases and, as a result, the activation of CREB via phosphorylation [21]. After 4 h of incubation, the resulting fluorescence is measured each hour for a 4 h period using an IX83 from Olympus (Tokyo, Japan). The resulting fluorescent images were evaluated using ImageJ 1.54b software.

### 2.4. Image Analysis

For each fluorophore present during confocal imaging, an own color channel image was acquired showing the excitation of either Hoechst 33342, Con A-Alexa Fluor™ 594 or the PMMA beads. The three channels were then merged via ImageJ. To analyze the intensity profiles after the stimulation of transfected HEK293 cells (see Section 2.3) with and without PMMA, a binary image was created which contains the intensity for each cell emitting light after excitation of MGFP. For each cell present in the image acquired, ImageJ determined the average intensity. The cutoff value of the pixel intensity to differentiate between background and cells was 5000. All objects smaller than  $90 \mu\text{m}^2$  were excluded from the evaluation. This allowed for sufficient differentiation between cells and background artefacts. Using RStudio 2023.09.1 (Posit PBS, Boston, MA, USA), boxplots were made showing the resulting average intensity of all cells for every time point with the corresponding standard deviation and number of cells detected.

### 2.5. Beads

Fluorescent PMMA beads were purchased from PolyAn (Berlin, Germany). The fluorophore "PolyAn Orange" was incorporated into the PMMA matrix during polymerization, preventing leaking. The beads were covered with carboxy groups, enabling coupling of proteins. Nanobeads with 165 nm diameter and microbeads with 2 µm diameter were used in this study.

## 3. Results

### 3.1. Confocal Imaging

Due to the accumulation of microplastics in the lungs and kidneys, cells within those organs are exposed to effects from the uptake of microplastics [22]. Published studies have shown a link between particles in the air and the development and increase in lung diseases [23]. There is a link between ingested polystyrene microparticles and kidney

damage in mice [24]. The selected cell lines are established and well-characterized. As previous literature indicates, HEK293 and A549 cells take up PMMA, whereas for MRC5, no literature regarding the uptake of PMMA can be found [13,25]. By visualizing whether PMMA beads enter the cytosol of the three cell lines, presumptions can be made regarding whether it is likely that PMMA will have an effect on signal transduction pathways of human cell lines.

Con A was used to stain the cell membrane, allowing for the visualization of the interface between the outside and inside of the cell. We were able to detect PMMA beads inside the cytosol of the HEK293, A549 and MRC5 cells (Figure 1). For each cell line analyzed, multiple beads entered the cell. The beads were randomly distributed within the cytosol. No PMMA beads were detected within the nucleus. The beads appeared yellow rather than green after merging all the color channels due to the mixing of the signals of the PMMA beads and Con A. This indicates that the beads were surrounded by a membrane structure. Interestingly, the beads located outside the cells also seemed to be surrounded by a membrane structure. Our data allow no discrimination of whether this is an artefact due to unspecific binding of Con A to the beads or if the beads were secreted by the cells during the staining process.

The size of the beads was determined using ImageJ and is shown in Table 1. Due to aggregation, the determined size of the nanobeads ( $\sim 0.6 \mu\text{m}$ ) differs by a factor of three from the starting material ( $\text{Ø} = 165 \text{ nm}$ ). While we cannot discriminate exactly at which point the aggregation occurred, it is highly likely the aggregation occurred prior to the cell entrance. The PMMA beads incubated with DMEM in the absence of cells already showed aggregation, indicating that the aggregation likely took place before their uptake by cells. The microbeads showed no aggregation, with size measurements averaging at  $2.03 \mu\text{m}$ .

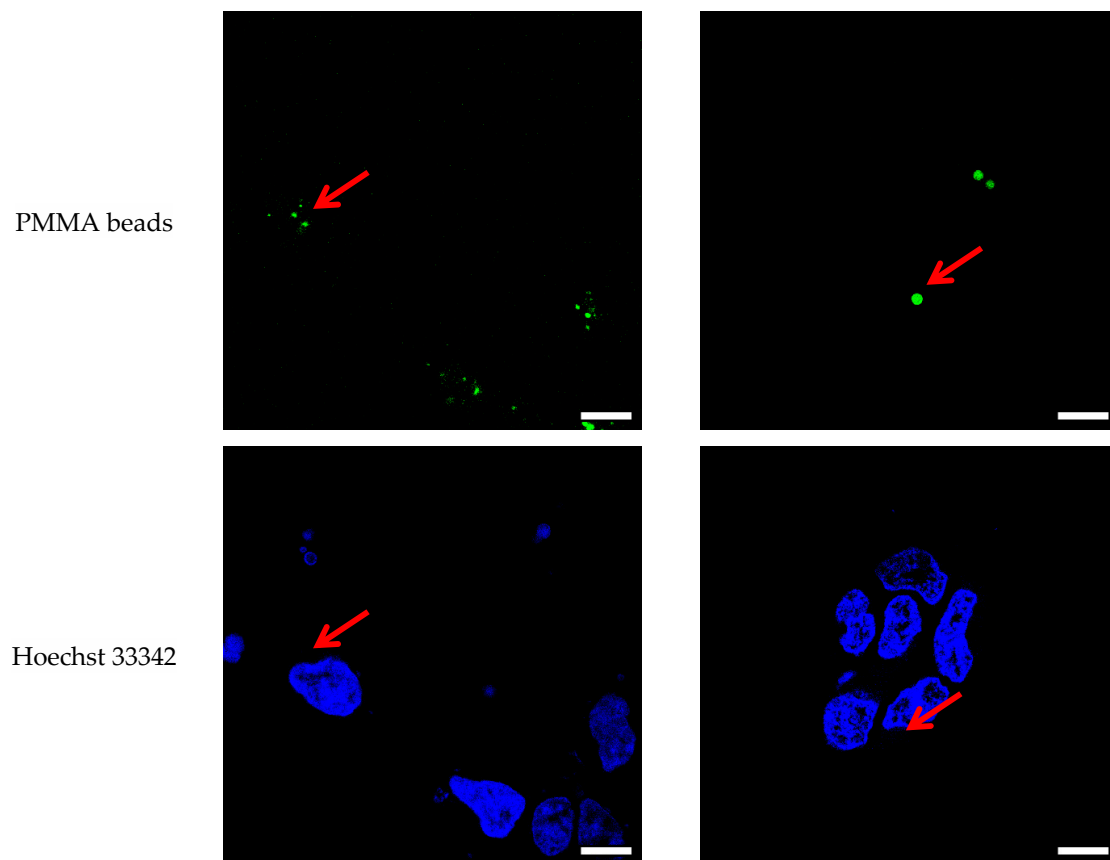


Figure 1. Cont.

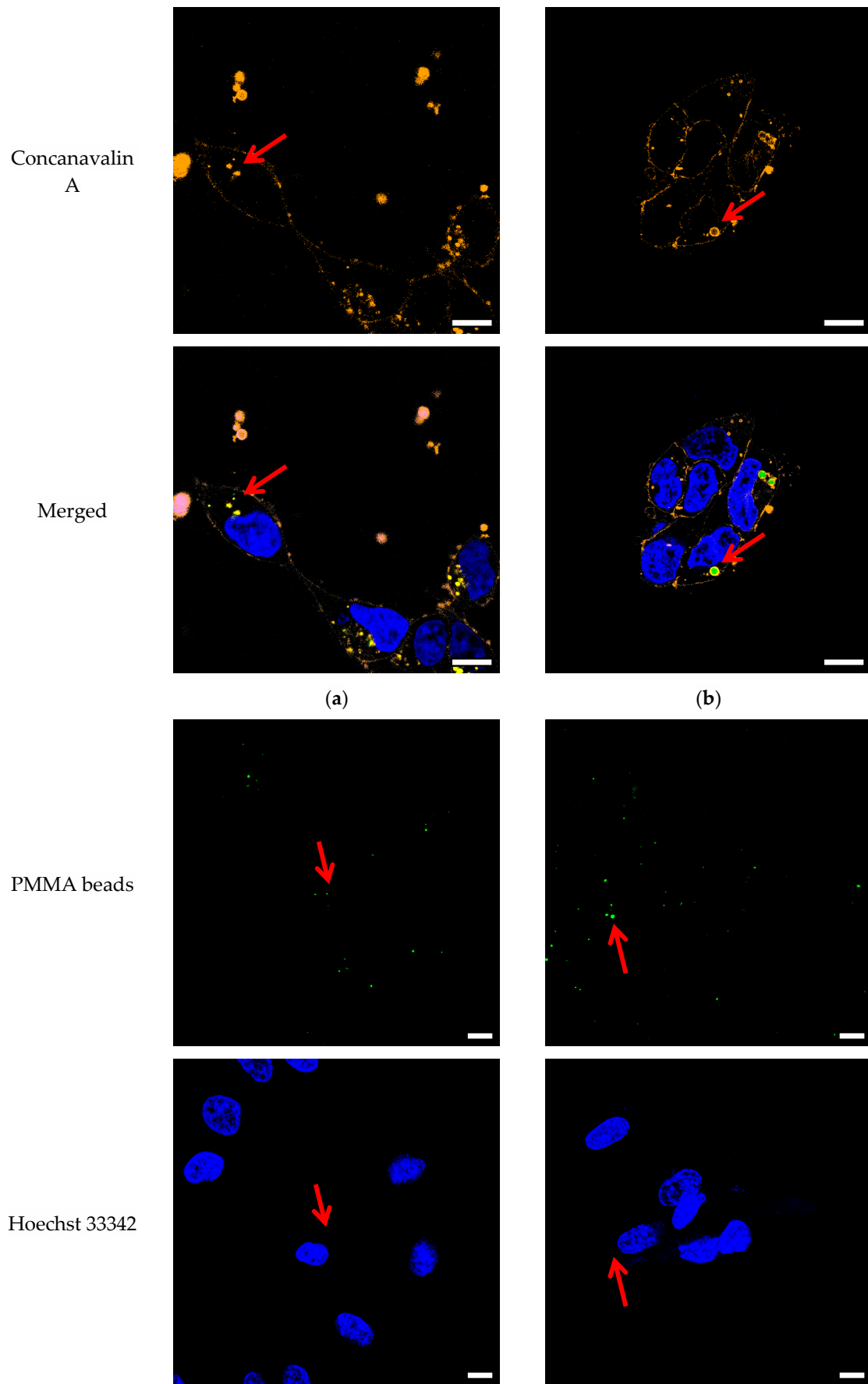
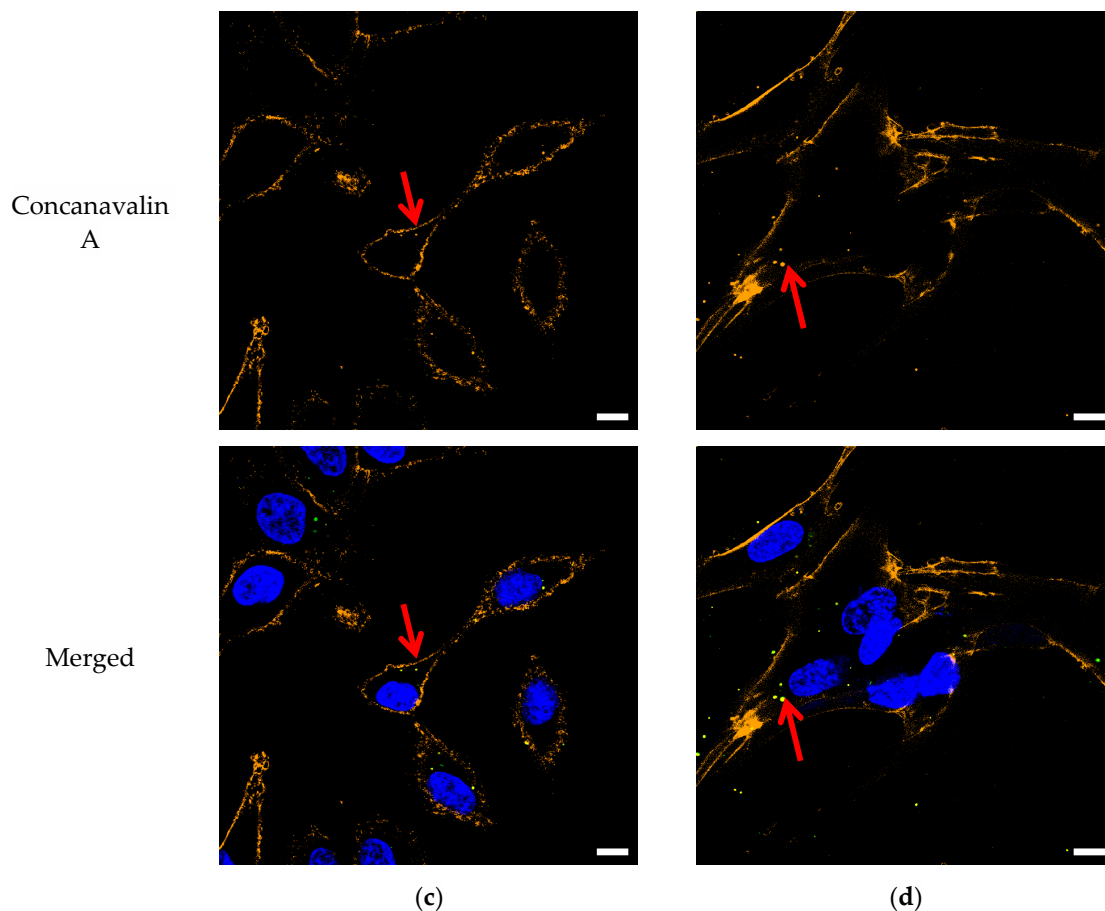


Figure 1. Cont.



**Figure 1.** Confocal images showing HEK293 (a,b), A549 (c) and MRC5 (d) cells after incubation for 48 h with polymethylmethacrylate (PMMA) beads (green). Concanavalin A (Con A)-Alexa Fluor™ 594 (orange) was used to visualize the cell membrane while Hoechst 33,342 was used as a nuclear stain (blue). In (a,c,d), cells were incubated with PMMA nanobeads ( $\text{\O} = 165 \text{ nm}$ ). In (b), cells were incubated with PMMA microbeads ( $\text{\O} = 2 \text{ }\mu\text{m}$ ). Red arrows indicate the position of PMMA. Scale bars represent  $10 \text{ }\mu\text{m}$ .

**Table 1.** Average size of green objects seen in Figure 1.

Figure	(a)	(b)	(c)	(d)
Cell line	HEK293	HEK293	A549	MRC5
Average size ( $\mu\text{m}$ ) determined	$0.54 \pm 0.29$	$2.03 \pm 0.19$	$0.76 \pm 0.27$	$0.66 \pm 0.47$
Average size ( $\mu\text{m}$ ) of the beads	0.165	2	0.165	0.165
Polydispersity Index	9.1%	8.9%	9.1%	9.1%

### 3.2. Doubling Time

The cells were incubated with varying amounts of PMMA for 72 h. After incubation, the cells were stained with Hoechst 33342. Using the fluorescence microscope IX83, images were acquired of the cells. ScanR, a processing software, allows for the determination of the number of cells after 72 h of incubation and therefore allows for the calculation of the doubling time  $t_0$ . The results are summarized in Table 2.

**Table 2.** Doubling time of HEK293, A549 and MRC5 cells after incubation with PMMA for 72 h ( $n = 3$ ).

Cell Line	$\emptyset$	Beads/mL	$t_0$ (h)
HEK293	165 nm	$4.5 \times 10^9$	$26.00 \pm 3.85$
		$4.5 \times 10^8$	$25.96 \pm 3.49$
		0	$27.44 \pm 2.33$
	2 $\mu\text{m}$	$2.53 \times 10^6$	$28.84 \pm 2.95$
		$2.53 \times 10^5$	$29.94 \pm 3.01$
		0	$29.56 \pm 2.75$
A549	165 nm	$4.5 \times 10^9$	$30.84 \pm 1.64$
		$4.5 \times 10^8$	$33.17 \pm 3.89$
		0	$29.86 \pm 1.62$
	2 $\mu\text{m}$	$2.53 \times 10^6$	$29.21 \pm 1.36$
		$2.53 \times 10^5$	$28.61 \pm 3.30$
		0	$29.44 \pm 2.76$
MRC5	165 nm	$4.5 \times 10^9$	$51.26 \pm 7.91$
		$4.5 \times 10^8$	$46.30 \pm 4.66$
		0	$45.44 \pm 4.37$
	2 $\mu\text{m}$	$2.53 \times 10^6$	$45.16 \pm 7.56$
		$2.53 \times 10^5$	$47.48 \pm 9.07$
		0	$46.25 \pm 7.32$

The doubling times of the HEK293, A549 and MRC5 cells incubated without the PMMA nano- and microbeads are in line with those found in other publications [26–28]. Only at excessively high particle densities exceeding environmentally relevant concentrations was a significant deviation in the doubling time measured. Under such conditions, the cells did not adhere to the growth surface and remained circular in suspension. Apart from that, the incubation with PMMA resulted in no significant reduction in cell growth or cell division or alteration in cell morphology. This indicates that PMMA shows no short-term toxicity towards the growth and division of HEK293, A549 and MRC5 cells.

### 3.3. Transfection of HEK 293 Cells

The plasmids used for transfection were derived from a reporter assay kit used for the quantitative assessment of signal transduction pathways. Previously, it has been shown that the addition of PMMA nanobeads will result in abolished in vitro gene expression [16]. Transfection using the same plasmids enables assessment of whether CREB-mediated signaling is altered in HEK293 cells due to the presence of PMMA as well. The resulting intensity after stimulation is shown in Figure 2. The HEK293 cells were transfected with CMV-MGFP as the positive control, CRE-MGFP as the reporter construct and TATA-MGFP linked to a non-inducible region as the negative control. Prior to transfection and stimulation, the cells were incubated with PMMA nanobeads ( $\emptyset = 165$  nm,  $4.5 \times 10^9$  beads/mL) or PBS for 72 h. By adding the nanobeads during cell seeding, the uptake of beads by the cells is ensured. Additionally, this will result in the sufficient distribution of the nanobeads between the cells, whereby the PMMA nanobeads will have entered most of the cells.

Incubation with the PMMA nanobeads ( $4.5 \times 10^9$  beads/mL) did not alter CREB-mediated cell signaling. For the CMV-MGFP (positive control) fluorescence intensity, prior incubation with PBS resulted in an average intensity of  $10,451 \pm 3401$  after 4 h with no significant changes over the course of the experiment. Incubation with the PMMA nanobeads resulted in a similar initial intensity of  $10,191 \pm 3787$ , while no significant changes were displayed over time either. The stimulation of the transfected HEK293 cells with the CRE-MGFP (reporter) showed an increase in the intensity measured over time independent of prior incubation with PBS or the PMMA nanobeads.

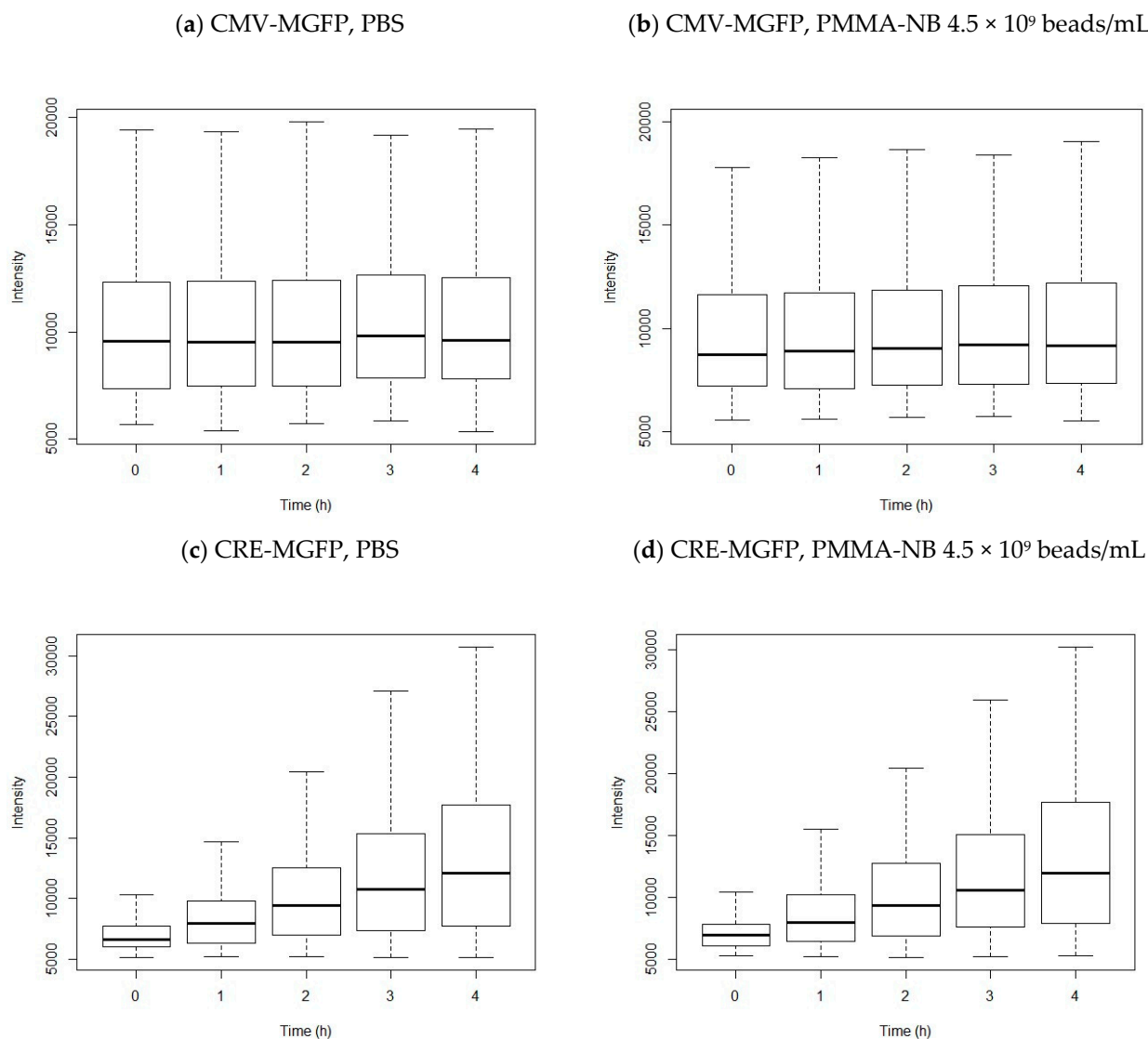


**Figure 2.** Quantification of cAMP response element binding protein (CREB)-mediated signaling in HEK293 cells after stimulation with forskolin and 3-Isobutyl-1-methylxanthin (IBMX). Prior to stimulation, cells in (a,b) were incubated with either PBS or PMMA nanobeads and then transfected with CMV-MGFP (positive control). Cells in (c,d) were also incubated with either PBS or PMMA nanobeads but then transfected using the CRE-MGFP (reporter). The standard deviation was calculated using RStudio. Table 3 shows the number of cells sufficient fluorescence and therefore being detected.

**Table 3.** Number of cells emitting sufficient fluorescence for detection after transfection and stimulation.

	0 h	1 h	2 h	3 h	4 h
CMV-MGFP, PBS	316	329	369	389	432
CMV-MGFP, PMMA-NB $4.5 \times 10^9$ beads/mL	299	343	376	423	491
CRE-MGFP, PBS	314	575	720	788	837
CRE-MGFP, PMMA-NB $4.5 \times 10^9$ beads/mL	323	551	701	781	794

The average intensity for incubation with PBS rose from  $7042 \pm 1605$  to  $13,136 \pm 6044$ , clearly showing the stimulation of the signaling pathway. Similarly, the intensity rose for

prior incubation with PMMA from  $7124 \pm 1350$  to  $13,096 \pm 5867$ . The data show CREB-mediated cell signaling through stimulation using forskolin and IBMX is not altered by prior incubation with PMMA nanobeads.

#### 4. Discussion

##### 4.1. Confocal Imaging

Since the surface of human cells is covered with glycoproteins and glycolipids, staining with fluorophore-coupled Con A allows for the visualization of the cell membrane via fluorescence microscopy. This allows for the determination of whether PMMA beads are within cells or outside, as the cell membrane serves as an interface between. HEK293, A549 and MRC5 cells uptake PMMA [13,25]. The images in Figure 1 show multiple beads located within the HEK293, A549 and MRC5 cells. The PMMA beads were randomly distributed within the cytosol of the cells. The size of the internalized PMMA nanobeads increased by a factor of three. This indicates aggregation occurring within the PMMA nanobeads. In a complex environment like biological media, nanoparticles tend to aggregate [29]. Therefore, the observed aggregation of the beads most likely takes place before their uptake by cells. During uptake, these aggregates remain intact and enter the cytosol. Since the signals of the PMMA beads overlap with those of Con A, the binding of Con A to the beads is proven. While the unspecific binding of Con A to the beads is possible, we propose the binding of Con A is specific due to protein adsorption to the beads prior to being internalized. Furthermore, previous reports suggest the uptake of PMMA beads is via endocytosis. During this process, the beads end up as late endosomes and lysosomes [30]. Lysosomes are embedded within a membrane containing glycoproteins on its surface; hence, the binding of Con A is observed [31]. Coincidentally, the size of the nanobead aggregates is within the usual size of lysosomes, ranging between 200 and 600 nm, further supporting that the mechanism behind the uptake of PMMA beads is endocytosis [32]. Regarding the PMMA microbeads (2  $\mu\text{m}$ ), no aggregation was observed after incubation with cells. The aggregation of nanobeads can be of relevance regarding drug delivery systems based on PMMA nanobeads, especially since the aggregation of intravenously administered nano-therapeutics results in an increased clearance in the liver [29]. Due to the fixation of cells necessary for fluorescence staining, the quantification of PMMA beads per cell was not possible in this experimental setup. Nonetheless, a dependency is detectable regarding the uptake of PMMA beads by HEK293, A549 and MRC5 cells. The larger the diameter of the beads, the smaller the number of beads taken up by each cell.

##### 4.2. Doubling Time

In accordance with other publications, the incubation of HEK293 and A549 cells with PMMA beads resulted in no significant reduction in the cells counted, with the doubling times remaining unaffected. No major effects of PMMA on cell growth, division or the cell cycle are reported [13,33,34]. No publication has been found regarding the cytotoxicity of PMMA towards MRC5. Our results indicate no major effects occur due to the doubling times not being altered by incubation with PMMA as well. The beads are split evenly between cells, with the distribution of the beads appearing to be random during cell division. Only by incubation with excessively high amounts of PMMA can a reduction in cell growth be seen. While the uptake of excessive amounts of PMMA by a human is unlikely, due to the local enrichment of microplastics in human organisms, local harmful effects cannot be excluded entirely. Since we only investigated the direct exposure of human cell lines to PMMA beads, no assumptions can be made regarding long-term toxicity.

##### 4.3. Transfection

The addition of 100  $\mu\text{g}/\text{mL}$  PMMA nanobeads abolishes CREB-mediated in vitro transcription using the same reporter assay as in this work [16]. In accordance with da Silva Brito et al., we concluded that a concentration of 12.5  $\mu\text{g}/\text{mL}$  [ $4.5 \times 10^9$  beads/ $\text{mL}$ ; 0.0125% ( $w/w$ )] is more appropriate in in vitro experiments, also resembling the average

microplastic concentration of 0.01% in marine environments [13,35]. While the concentration in blood samples is significantly lower, at 1.6 µg/mL, due to the accumulation within the lungs and kidneys, we expect a local increase in plastics in these organs supporting the chosen concentration [36]. With HEK293 cells able to internalize PMMA nanobeads, we expected similar effects within the cells. Regarding the cells transfected with the CMV-MGFP plasmid, the constitutive expression of MGFP is not altered. Since nanobeads are not entering the cell nucleus after internalization, no inhibition of transcription can occur. Nevertheless, internalized microplastics can alter cellular structures and interact with proteins resulting in conformational changes in the protein secondary structure and loss of function [37]. This is heavily influenced by the surface composition of the microplastic though, influencing its biological fate and toxicity [38]. The aggregation and uptake of PMMA beads via endocytosis results in the beads being embedded in a membrane. Due to this, no alteration regarding the translation of MGFP within the cytosol is given after uptake by HEK293 cells either. Furthermore, the transfection of HEK293 cells with the CRE-MGFP plasmid and the stimulation of PKA signaling pathways via forskolin and IBMX are not altered by the presence of PMMA nanobeads within the cytosol either. The resulting expression of MGFP remains unaffected when comparing that of cells priorly incubated with PBS to cells incubated with PMMA nanobeads. These results underline the role the surface composition plays regarding the toxicity of microplastics in general. While *in vitro* transcription can be abolished by adding PMMA beads, no equivalent alteration is found within HEK293 cells. This implies that after the uptake by HEK293 cells, the PMMA nanobeads lose the ability to alter cell signaling via loss of function for essential proteins. While a connection between neurodegenerative disorders and the uptake of microplastics is likely, we found no evidence that the internalization of PMMA nanobeads interfering with CREB-mediated signaling pathways plays a role in that for the cell lines tested.

Microplastics on land and in the sea are continuously in contact with a complex biological environment exposed to constant physical and chemical changes. For risk assessment regarding human health, the relationship between the biological environment, chemical degradation and aging resulting in changes in the surface composition of microplastics needs to be determined. Understanding the role the surface composition plays is key for a better understanding of the toxicity of internalized microplastics.

**Author Contributions:** A.B. and H.S. designed the experiments. A.B. performed the experiments. A.B. wrote the paper together with H.S. All authors discussed the results and commented on the manuscript. All authors have read and agreed to the published version of the manuscript.

**Funding:** This research received no external funding.

**Institutional Review Board Statement:** Not applicable.

**Informed Consent Statement:** Not applicable.

**Data Availability Statement:** The data presented in this study are available on request from the corresponding author.

**Acknowledgments:** We would like to thank Ralph Gräf from the University of Potsdam for allowing the usage of the confocal microscope.

**Conflicts of Interest:** The authors declare no conflicts of interest.

## References

1. Geyer, R.; Jambeck, J.R.; Law, K.L. Production, Use, and Fate of All Plastics Ever Made. *Sci. Adv.* **2017**, *3*, e1700782. [[CrossRef](#)] [[PubMed](#)]
2. Moore, C.J. Synthetic Polymers in the Marine Environment: A Rapidly Increasing, Long-Term Threat. *Environ. Res.* **2008**, *108*, 131–139. [[CrossRef](#)] [[PubMed](#)]
3. Hidalgo-Ruz, V.; Gutow, L.; Thompson, R.C.; Thiel, M. Microplastics in the Marine Environment: A Review of the Methods Used for Identification and Quantification. *Environ. Sci. Technol.* **2012**, *46*, 3060–3075. [[CrossRef](#)]
4. Yokota, K.; Waterfield, H.; Hastings, C.; Davidson, E.; Kwietniewski, E.; Wells, B. Finding the Missing Piece of the Aquatic Plastic Pollution Puzzle: Interaction between Primary Producers and Microplastics. *Limnol. Oceanogr. Lett.* **2017**, *2*, 91–104. [[CrossRef](#)]

5. Caruso, G. Microplastics as Vectors of Contaminants. *Mar. Pollut. Bull.* **2019**, *146*, 921–924. [[CrossRef](#)] [[PubMed](#)]
6. Xiang, C.; Chen, H.; Liu, X.; Dang, Y.; Li, X.; Yu, Y.; Li, B.; Li, X.; Sun, Y.; Ding, P.; et al. UV-Aged Microplastics Induces Neurotoxicity by Affecting the Neurotransmission in Larval Zebrafish. *Chemosphere* **2023**, *324*, 138252. [[CrossRef](#)] [[PubMed](#)]
7. Qiao, R.; Sheng, C.; Lu, Y.; Zhang, Y.; Ren, H.; Lemos, B. Microplastics Induce Intestinal Inflammation, Oxidative Stress, and Disorders of Metabolome and Microbiome in Zebrafish. *Sci. Total Environ.* **2019**, *662*, 246–253. [[CrossRef](#)] [[PubMed](#)]
8. Vaishya, R.; Chauhan, M.; Vaish, A. Bone Cement. *J. Clin. Orthop. Trauma* **2013**, *4*, 157–163. [[CrossRef](#)]
9. Becker, L.C.; Bergfeld, W.F.; Belsito, D.V.; Hill, R.A.; Klaassen, C.D.; Liebler, D.C.; Marks, J.G.; Shank, R.C.; Slaga, T.J.; Snyder, P.W.; et al. Final Report of the Cosmetic Ingredient Review Expert Panel Safety Assessment of Polymethyl Methacrylate (PMMA), Methyl Methacrylate Crosspolymer, and Methyl Methacrylate/Glycol Dimethacrylate Crosspolymer. *Int. J. Toxicol.* **2011**, *30*, 54S–65S. [[CrossRef](#)]
10. Gad, M.; Fouada, S.; Al-Harbi, F.; Nöpänkangas, R.; Raustia, A. PMMA Denture Base Material Enhancement: A Review of Fiber, Filler, and Nanofiller Addition. *Int. J. Nanomedicine* **2017**, *12*, 3801–3812. [[CrossRef](#)]
11. Lin, M.; Wang, H.; Meng, S.; Zhong, W.; Li, Z.; Cai, R.; Chen, Z.; Zhou, X.; Du, Q. Structure and Release Behavior of PMMA/Silica Composite Drug Delivery System. *J. Pharm. Sci.* **2007**, *96*, 1518–1526. [[CrossRef](#)] [[PubMed](#)]
12. Prabakaran, S.; Jeyaraj, M.; Nagaraj, A.; Sadasivuni, K.K.; Rajan, M. Polymethyl Methacrylate–Ovalbumin@Graphene Oxide Drug Carrier System for High Anti-Proliferative Cancer Drug Delivery. *Appl. Nanosci.* **2019**, *9*, 1487–1500. [[CrossRef](#)]
13. Da Silva Brito, W.A.; Singer, D.; Miebach, L.; Saadati, F.; Wende, K.; Schmidt, A.; Bekeschus, S. Comprehensive in Vitro Polymer Type, Concentration, and Size Correlation Analysis to Microplastic Toxicity and Inflammation. *Sci. Total Environ.* **2023**, *854*, 158731. [[CrossRef](#)]
14. Yang, Y.-F.; Chen, C.-Y.; Lu, T.-H.; Liao, C.-M. Toxicity-Based Toxicokinetic/Toxicodynamic Assessment for Bioaccumulation of Polystyrene Microplastics in Mice. *J. Hazard. Mater.* **2019**, *366*, 703–713. [[CrossRef](#)]
15. Pironti, C.; Notarstefano, V.; Ricciardi, M.; Motta, O.; Giorgini, E.; Montano, L. First Evidence of Microplastics in Human Urine, a Preliminary Study of Intake in the Human Body. *Toxics* **2022**, *11*, 40. [[CrossRef](#)]
16. Pellegrino, A.; Danne, D.; Weigel, C.; Seitz, H. An In Vitro Assay to Quantify Effects of Micro- and Nano-Plastics on Human Gene Transcription. *Microplastics* **2023**, *2*, 122–131. [[CrossRef](#)]
17. Kida, S.; Serita, T. Functional Roles of CREB as a Positive Regulator in the Formation and Enhancement of Memory. *Brain Res. Bull.* **2014**, *105*, 17–24. [[CrossRef](#)]
18. Oike, Y.; Takakura, N.; Hata, A.; Kaname, T.; Akizuki, M.; Yamaguchi, Y.; Yasue, H.; Araki, K.; Yamamura, K.; Suda, T. Mice Homozygous for a Truncated Form of CREB-Binding Protein Exhibit Defects in Hematopoiesis and Vasculo-Angiogenesis. *Blood* **1999**, *93*, 2771–2779. [[CrossRef](#)] [[PubMed](#)]
19. Saura, C.A.; Valero, J. The Role of CREB Signaling in Alzheimer’s Disease and Other Cognitive Disorders. *Revneuro* **2011**, *22*, 153–169. [[CrossRef](#)]
20. Shapiro, L.; Katchur, N. Microplastic Exposure and the of Parkinson’s Disease: The Effects of Microplastics in the Body and Similarities to the Pathogenesis of Parkinson’s Disease. *J. Stud. Res.* **2023**, *11*. [[CrossRef](#)]
21. Thompson, R.; Casali, C.; Chan, C. Forskolin and IBMX Induce Neural Transdifferentiation of MSCs Through Downregulation of the NRSF. *Sci. Rep.* **2019**, *9*, 2969. [[CrossRef](#)]
22. Pitt, J.A.; Kozal, J.S.; Jayasundara, N.; Massarsky, A.; Trevisan, R.; Geitner, N.; Wiesner, M.; Levin, E.D.; Di Giulio, R.T. Uptake, Tissue Distribution, and Toxicity of Polystyrene Nanoparticles in Developing Zebrafish (Danio Rerio). *Aquat. Toxicol.* **2018**, *194*, 185–194. [[CrossRef](#)] [[PubMed](#)]
23. Van Dijk, F.; Van Eck, G.; Cole, M.; Salvati, A.; Bos, S.; Gosens, R.; Melgert, B. Exposure to Textile Microplastic Fibers Impairs Epithelial Growth. *Eur. Respir. J.* **2020**, *56*, 1972. [[CrossRef](#)]
24. Meng, X.; Zhang, J.; Wang, W.; Gonzalez-Gil, G.; Vrouwenvelder, J.S.; Li, Z. Effects of Nano- and Microplastics on Kidney: Physicochemical Properties, Bioaccumulation, Oxidative Stress and Immunoreaction. *Chemosphere* **2022**, *288*, 132631. [[CrossRef](#)] [[PubMed](#)]
25. Adinolfi, B.; Pellegrino, M.; Tombelli, S.; Trono, C.; Giannetti, A.; Domenici, C.; Varchi, G.; Sotgiu, G.; Ballestri, M.; Baldini, F. Polymeric Nanoparticles Promote Endocytosis of a Survivin Molecular Beacon: Localization and Fate of Nanoparticles and Beacon in Human A549 Cells. *Life Sci.* **2018**, *215*, 106–112. [[CrossRef](#)] [[PubMed](#)]
26. Jacobs, J.P.; Jones, C.M.; Baille, J.P. Characteristics of a Human Diploid Cell Designated MRC-5. *Nature* **1970**, *227*, 168–170. [[CrossRef](#)] [[PubMed](#)]
27. Russell, W.C.; Graham, F.L.; Smiley, J.; Nairn, R. Characteristics of a Human Cell Line Transformed by DNA from Human Adenovirus Type 5. *J. Gen. Virol.* **1977**, *36*, 59–72. [[CrossRef](#)]
28. Assanga, I. Cell Growth Curves for Different Cell Lines and Their Relationship with Biological Activities. *Int. J. Biotechnol. Mol. Biol. Res.* **2013**, *4*, 60–70. [[CrossRef](#)]
29. Moore, T.L.; Rodriguez-Lorenzo, L.; Hirsch, V.; Balog, S.; Urban, D.; Jud, C.; Rothen-Rutishauser, B.; Lattuada, M.; Petri-Fink, A. Nanoparticle Colloidal Stability in Cell Culture Media and Impact on Cellular Interactions. *Chem. Soc. Rev.* **2015**, *44*, 6287–6305. [[CrossRef](#)]
30. Vollrath, A.; Schallon, A.; Pietsch, C.; Schubert, S.; Nomoto, T.; Matsumoto, Y.; Kataoka, K.; Schubert, U.S. A Toolbox of Differently Sized and Labeled PMMA Nanoparticles for Cellular Uptake Investigations. *Soft Matter* **2013**, *9*, 99–108. [[CrossRef](#)]

31. Saftig, P.; Klumperman, J. Lysosome Biogenesis and Lysosomal Membrane Proteins: Trafficking Meets Function. *Nat. Rev. Mol. Cell Biol.* **2009**, *10*, 623–635. [[CrossRef](#)] [[PubMed](#)]
32. Barral, D.C.; Staiano, L.; Guimas Almeida, C.; Cutler, D.F.; Eden, E.R.; Futter, C.E.; Galione, A.; Marques, A.R.A.; Medina, D.L.; Napolitano, G.; et al. Current Methods to Analyze Lysosome Morphology, Positioning, Motility and Function. *Traffic* **2022**, *23*, 238–269. [[CrossRef](#)] [[PubMed](#)]
33. Khan, F.A.; Akhtar, S.; Almohazey, D.; Alomari, M.; Almofty, S.A.; Badr, I.; Elaissari, A. Targeted Delivery of Poly (Methyl Methacrylate) Particles in Colon Cancer Cells Selectively Attenuates Cancer Cell Proliferation. *Artif. Cells Nanomedicine Biotechnol.* **2019**, *47*, 1533–1542. [[CrossRef](#)] [[PubMed](#)]
34. Feuser, P.E.; Gaspar, P.C.; Ricci-Júnior, E.; Silva, M.C.S.D.; Nele, M.; Sayer, C.; De Araújo, P.H.H. Synthesis and Characterization of Poly(Methyl Methacrylate) PMMA and Evaluation of Cytotoxicity for Biomedical Application. *Macromol. Symp.* **2014**, *343*, 65–69. [[CrossRef](#)]
35. Everaert, G.; Van Cauwenberghe, L.; De Rijcke, M.; Koelmans, A.A.; Mees, J.; Vandegheuchte, M.; Janssen, C.R. Risk Assessment of Microplastics in the Ocean: Modelling Approach and First Conclusions. *Environ. Pollut.* **2018**, *242*, 1930–1938. [[CrossRef](#)] [[PubMed](#)]
36. Leslie, H.A.; Van Velzen, M.J.M.; Brandsma, S.H.; Vethaak, A.D.; Garcia-Vallejo, J.J.; Lamoree, M.H. Discovery and Quantification of Plastic Particle Pollution in Human Blood. *Environ. Int.* **2022**, *163*, 107199. [[CrossRef](#)] [[PubMed](#)]
37. Windheim, J.; Colombo, L.; Battajni, N.C.; Russo, L.; Cagnotto, A.; Diomede, L.; Bigini, P.; Vismara, E.; Fiumara, F.; Gabbrielli, S.; et al. Micro- and Nanoplastics' Effects on Protein Folding and Amyloidosis. *Int. J. Mol. Sci.* **2022**, *23*, 10329. [[CrossRef](#)]
38. Wang, J.; Cong, J.; Wu, J.; Chen, Y.; Fan, H.; Wang, X.; Duan, Z.; Wang, L. Nanoplastic-Protein Corona Interactions and Their Biological Effects: A Review of Recent Advances and Trends. *TrAC Trends Anal. Chem.* **2023**, *166*, 117206. [[CrossRef](#)]

**Disclaimer/Publisher's Note:** The statements, opinions and data contained in all publications are solely those of the individual author(s) and contributor(s) and not of MDPI and/or the editor(s). MDPI and/or the editor(s) disclaim responsibility for any injury to people or property resulting from any ideas, methods, instructions or products referred to in the content.